Supplementary Materials

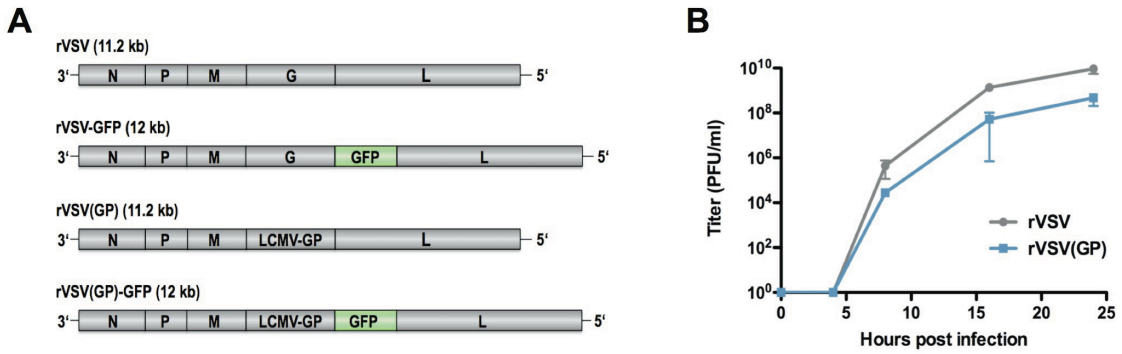

Fig. S1. Schematic representation of the recombinant vesicular stomatitis virus (VSV) genomes and its replication potential. (**A**) Genomes and the respective open reading frames are presented in 3'-5' orientation. (**B**) BHK-21 cells were infected with either rVSV or rVSV(GP) at an MOI of 0.1 and supernatants were sampled at the respective time-points post-infection. Data points represent titers as mean±SD of n=2 experiments.

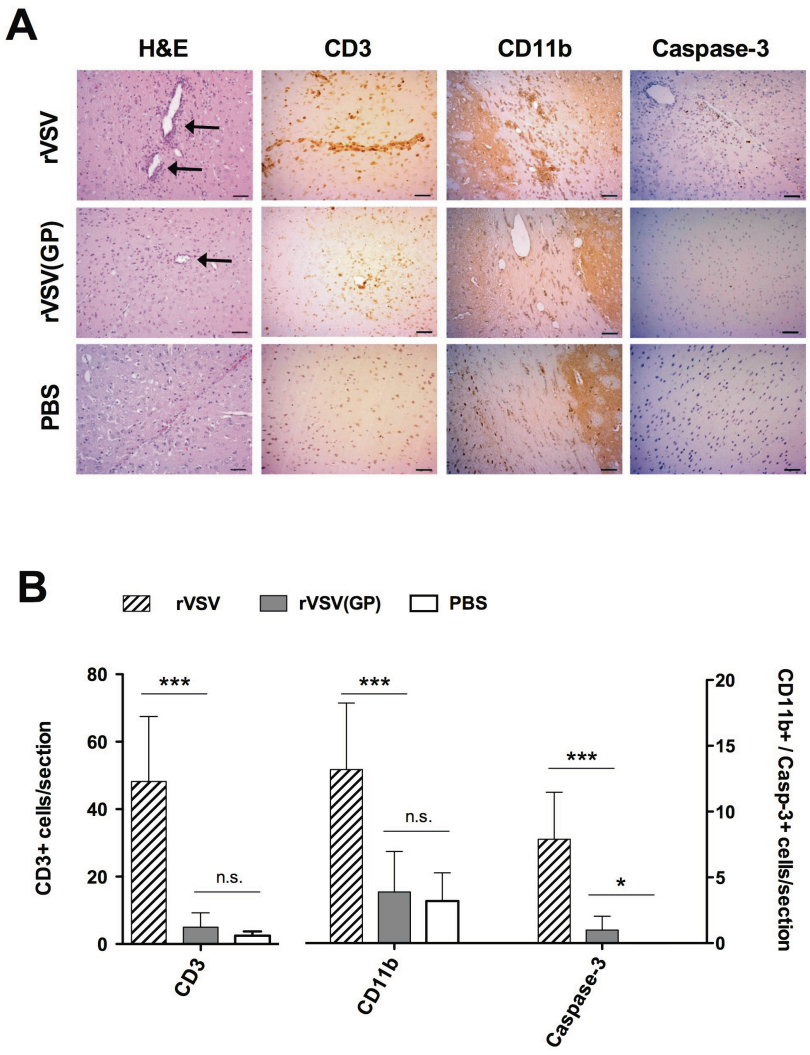

Fig. S2. rVSV(GP) administration i.c. is associated with marginal inflammation. CD-1 mice (n=3 per cohort) were injected i.c. with either 10^7 PFU rVSV(GP)-GFP-, 10 PFU rVSV-GFP or PBS. Mice were sacrificed at 3 dpi, coronal brain sections were prepared and inflammatory as well as apoptotic parameters were evaluated. (**A**) Representative micrographs of H&E stained, CD3, CD11b and cleaved caspase-3 stained sections are shown. (**B**) Quantification of $CD3^+$, $CD11b^+$ as well as cleaved caspase-3^+ cells. Bars represent mean±SD of 10 analyzed sections; *, $P<0.05$; ***, $P<0.001$; arrows indicate accumulation of lymphocytes around blood vessels; scale bar = 50 µm

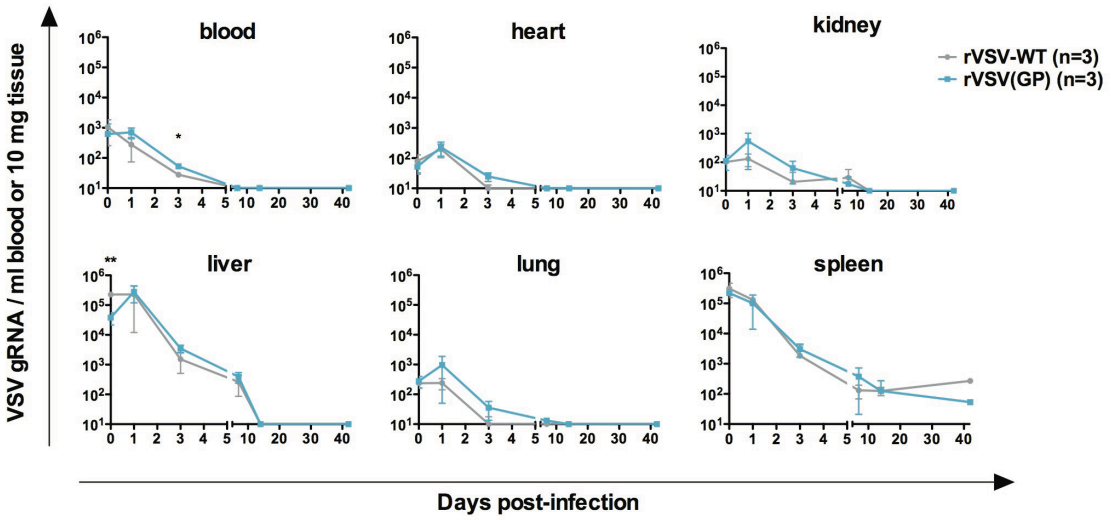

Fig. S3. rVSV(GP) tissue distribution after systemic application is almost consistent with rVSV. CD-1 mice (n=3/cohort and time-point) were injected i.v. with either 10^8 rVSV(GP), rVSV or PBS. At each indicated time-point n=3 animals/cohort were sacrificed. RNA was purified from whole blood and the respective organs. VSV genomic RNA (gRNA) levels were determined by reverse transcription real-time PCR and referenced against blood volume or tissue weight. gRNA kinetics in blood and all major organs is shown with individual data points representing mean±SD; *P<0.05; **, P<0.01

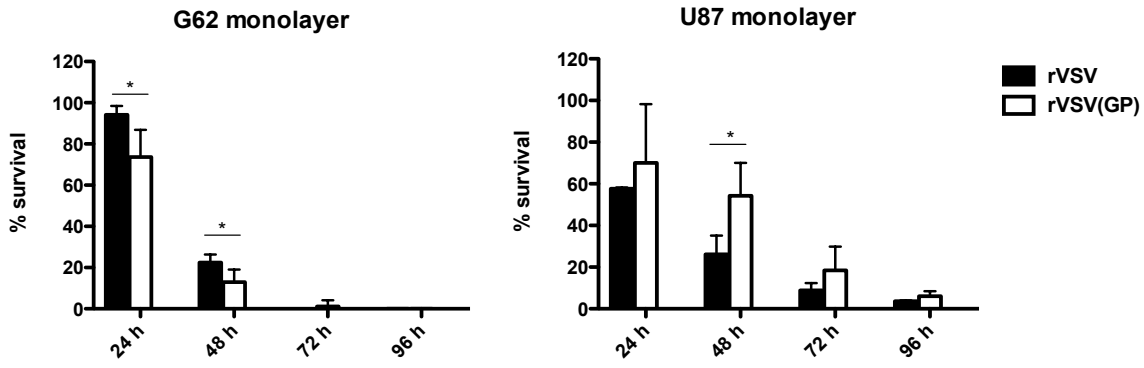

Fig. S4. rVSV(GP) is comparable to rVSV with regard to its *in vitro* antitumour efficacy. G62 and U87 human glioblastoma cells were grown as monolayers. Cultures were infected with rVSV(GP) or rVSV at an MOI of 0.1. Cell viability way assayed at the indicated time points post-infection via WST-1 assay compared to untreated controls. Bars represent mean±SD of n=3 independent experiments performed in dodecaplicates; *, $P<0.05$

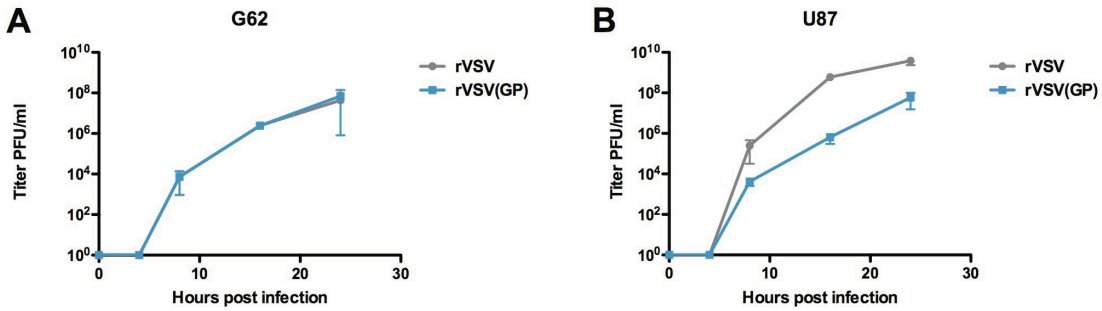

Fig. S5. Replication fitness of rVSV(GP) vs. rVSV in glioma cells. (**A**) G62 and (**B**) U87 human glioma cells were infected with either rVSV or rVSV(GP) at an MOI of 0.1. Supernatants were sampled at the respective time-points post-infection. Viral titers were determined on BHK-21 cells. Data points represent titers as mean±SD of n=2 experiments.

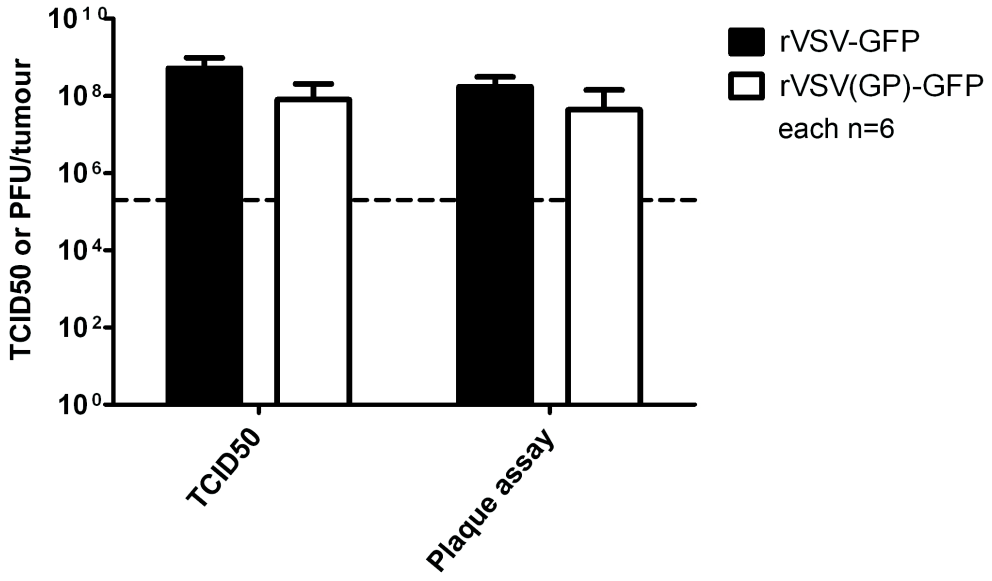

Fig. S6. Intratumoural virus administration in s.c. G62 human glioblastoma xenografts leads to productive infection and massive viral burst. 2x10^5 PFUs rVSV(GP)-GFP or rVSV-GFP were injected i.t. into s.c. bilateral G62 human glioblastoma xenografts in immunodeficient mice once the tumours reached a volume of 0.1 cm^3 (n=6 tumours per virus). At 3 days post-infection, animals were euthanized and tumours were explanted. Tumour tissue homogenates were generated and analyzed by $TCID_{50}$ and plaque assay on BHK-21 cells. Bars represent mean±SD of n=6 tumours; dashed line = viral input dose

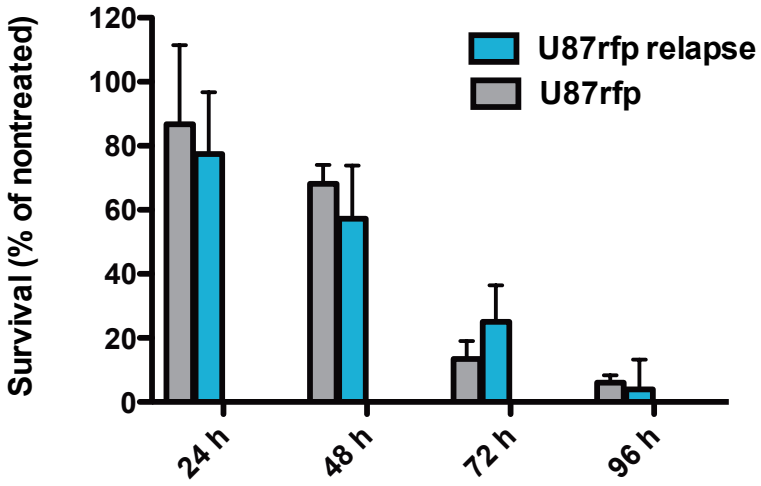

Fig. S7. U87rfp tumour relapse was not due to OV therapy resistance. U87-RFP cells as well as U87-RFP-relapse cells, established from recurrent tumour mass, were infected with rVSV(GP) at an MOI of 0.1. Cell viability was assayed at the indicated time points post-infection via WST-1 assay compared to untreated controls. Bars represent mean±SD of n=3 independent experiments performed in dodecaplicates